Dalton Transactions

Accepted Manuscript

Journal Name

ARTICLE

Two S = 1/2 One-Dimensional Barium Copper Phosphates Showing Antiferromagnetic and Ferromagnetic Intrachain Interactions†

Received 00th January 20xx,
Accepted 00th January 20xx

DOI: 10.1039/x0xx00000x

www.rsc.org/

Ming Yang,[a] Meiyan Cui,[a,b] Suyun Zhang,[a] Hongping Xiang,*[a] Wenbin Guo[a] and Zhangzhen He*[a]

Two barium copper phosphates, $BaCu_2(PO_4)_2(H_2O)$ (**1**) and $Ba_2Cu(HPO_4)(PO_4)(OH)$ (**2**), were synthesized under mild hydrothermal condition. The Cu cation in **1** adopts a $CuO_4(H_2O)$ square pyramidal coordination configuration, forming alternating chains along *b* axis through alternative corner and edge sharing, while the geometry of Cu center in **2** is a $CuO_4(OH)_2$ octahedron which further connects each other by edge sharing to constitute uniform chains along *b* axis. Magnetic behaviors of both compounds were analyzed by susceptibility, magnetization and heat capacity measurements. The dominant intrachain couplings are antiferromagnetic in **1** with a long-range ordering at 14 K and ferromagnetic in **2** without long-range ordering above 2 K. The first principle calculations indicate that the intrachain ferromagnetic couplings in **2** originate from Cu(1)–O(7)H–Cu(1) d$p\sigma$ correlation superexchanges. The susceptibility data of compounds **1** and **2** are fitted by using suitable antiferromagnetic chain and ferromagnetic chain models, respectively. In addition, we report results of infrared and thermal measurements of both compounds.

1 Introduction

The theoretical and experimental studies of one-dimensional (1D) quantum magnetic systems are extremely active.[1] Most investigations in these systems are focused on transition-metal oxides, especially for cuprates (Cu^{2+} with S = 1/2) because of strong quantum fluctuation and the discovery of high-temperature superconductivity.[2] In general, the geometries of Cu^{2+} centre are in the range of square, square-pyramid and octahedron. The $[CuO_n]$ (n = 4, 5 and 6) polyhedra are connected each other through corner and edge sharing, leading to various types of 1D structures, such as uniform chain,[3] alternating chain,[4] diamond chain[5] and ladder.[6] These features result in many fascinating magnetic properties, such as spin-Peierls transition,[3a] spin-singlet state with a finite gap[3b,4a,6b] and magnetization plateau.[4c,5a] For understanding those intriguing magnetic phenomena, analysis of intrachain and interchain exchange interactions is of vital importance.

Phosphate compounds have been widely investigated due to their rich crystal structures and numerous applications in the fields of adsorption, optics, energy and catalysis.[7] In the field of magnetism, the copper phosphate materials, particularly the utilization of alkaline earth metal ions and Pb^{2+} as counterions, formulating as $A_3Cu_3(PO_4)_4$ (A = Ca, Sr and Pb),[8] $ACu_2(PO_4)_2$ (A = Sr, Ba and Pb),[9] $A_2Cu(PO_4)_2$ (A = Sr and Ba)[10] and $ACuP_2O_7$ (A = Ca, Sr, Ba and Pb),[11] have received particular consideration owing to their nature of low-dimensionality. In Ba–Cu–P–O system constructed by 1D chains, for example, $BaCu_2(PO_4)_2$ feature isolated zigzag chains and shows a broad peak around 65 K,[9a,9b] while $Ba_2Cu(PO_4)_2$ contains $[Cu(PO_4)_2]$ uniform chains exhibiting short-range ordering at 82 K.[10a,10c] $BaCuP_2O_7$ consists of excellent 1D antiferromagnetic (AFM) linear chains with a broad maximum at 66.1 K and a long-range ordering at 0.81 K.[12] It is noted that the intrachain interactions between Cu neighbors are AFM. No ferromagnetic (FM) exchange is observed in this system. To date, a number of 1D FM hybrid organic–inorganic compounds based on Cu^{2+} chains have been synthesized,[13] and some of materials built from 1D FM Cu^{2+} chains have been reported in pure inorganic systems, such as $ACuV_2O_7$ (A = Sr and Ba)[14] and $BaCu_2Ge_3O_9{\cdot}H_2O$.[15]

For ongoing search new compounds in Ba–Cu–P–O system, we adopt hydrothermal method which can introduce water molecule and hydroxyl to framework and has been extensively used to prepare novel low-dimensional materials.[16] Herein, we report two barium copper phosphates, $BaCu_2(PO_4)_2(H_2O)$ (**1**) and $Ba_2Cu(HPO_4)(PO_4)(OH)$ (**2**), by one-pot method under mild hydrothermal condition. Both compounds are characterized by single crystal X-ray diffraction, infrared spectroscopy, thermal analysis, magnetic and specific heat measurements. The remarkable structural feature is alternating chains in **1** and uniform chains in **2**. We analyze magnetic coupling pathways and obtain intrachain exchange constants of both compounds by using suitable theoretical model. Moreover, the structures

[a] *State Key Laboratory of Structural Chemistry, Fujian Institute of Research on the Structure of Matter, Chinese Academy of Sciences, Fuzhou, 350002, P. R. China. E-mail: xianghp@fjirsm.ac.cn, hcz1988@hotmail.com, hezz@fjirsm.ac.cn. Fax: +86-591-63173255; Tel: +86-591-63173254; +86-591-63173255.*
[b] *University of Chinese Academy of Sciences, Beijing, 100049, P. R. China.*
†Electronic Supplementary Information (ESI) available: Tables of selected bond lengths and angles and atomic site parameters, Figs. S1-11, crystallographic files in CIF format. ICSD 430101 for **2**. See DOI: 10.1039/x0xx00000x.

and magnetisms of **1** and **2** are compared with those of corresponding anhydrous compounds.

2 Experimental

2.1 Materials and measurement

All chemical reagents were commercially available and used as received. Infrared spectra were measured on a VERTEX70 Fourier transform infrared spectrometry (FT-IR) spectrophotometer with KBr pellets in the range 350–4500 cm^{-1}. Thermogravimetry analyses (TGA) were performed on a Netzsch STA449C instrument from 25 to 1000 ˚C with a heating rate of 10 K/min under N_2 atmosphere. Powder X-ray diffraction (PXRD) were carried out by a Rigaku SCXmini X-ray diffractometer using Cu-*Kα* radiation with a scan speed of 5° min^{-1} and 2θ in the range of 5–65°. The direct-current magnetic susceptibility data of powder samples were collected on a Quantum Design MPMS-XL SQUID magnetometer between 2 and 300 K. Isothermal magnetization recorded at 2 K and specific heat curves measured from 300 to 4.5 K at zero magnetic field were conducted on a commercial Quantum Design PPMS.

2.2 Synthesis

Single crystals of **1** and **2** were obtained under one-pot hydrothermal condition. $BaCl_2·2H_2O$ (0.5 mmol, 0.1227 g), $CuCl_2·2H_2O$ (1 mmol, 0.1705 g) and H_3PO_4 (≥ 85%, 1.5 mmol, 0.1729 g) was dissolved in 8 mL H_2O. The mixture was transferred into a 28 mL Teflonlined autoclave. Then, 0.5 mL pyridine was added to the mixture. The reaction was heated to 160 °C for 72 h. After cooling to room temperature in 20 h, the product contains abundant of blue rhombus crystals (compound **1**) and a few of green block crystals (compound **2**). **1** and **2** were separated under microscope by manual.

2.3 X-Ray crystallography

Single crystal X-ray diffraction intensities of two compounds were collected on a Rigaku Mercury CCD diffractometer using graphite monochromatic Mo *Kα* radiation (λ = 0.71073 Å). Empirical absorption corrections were applied. The structures were solved with direct method and refined with a full-matrix least-squares technique on F^2 with the *SHELXTL* program package.[17] Anisotropic displacement parameters were assigned to all non-hydrogen atoms. The position of hydrogen atoms in compounds **1** and **2** were found from difference Fourier map The crystallographic details, for **1** and **2**, are compiled in Table 1, while selected bond lengths and angles and atomic site parameters are given in Tables S1 and S2.†

Table 1 The structure parameters and refinement results for $BaCu_2(PO_4)_2(H_2O)$ and $Ba_2Cu(HPO_4)(PO_4)(OH)$.

Compound	$BaCu_2(PO_4)_2(H_2O)$	$Ba_2Cu(HPO_4)(PO_4)(OH)$
Formula weight	472.38	546.16
Crystal system	orthorhombic	monoclinic
Space group	$P2_12_12_1$	$P2_1/m$
T (K)	293 (2)	293 (2)
a (Å)	5.163 (2)	8.328 (6)
b (Å)	9.730 (4)	5.868 (4)
c (Å)	14.574 (6)	9.078 (6)
α (°)	90	90
β (°)	90	112.57 (3)
γ (°)	90	90
V ($Å^3$)	732.2 (5)	409.6 (5)
Z	4	2
Density (g/cm^3)	4.285	4.427
Crystal size (mm^3)	0.35 × 0.26 × 0.20	0.16 × 0.11 × 0.09
Reflns collected	5589	4190
Unique reflns	1661	1027
R_{int}	0.022	0.024
$R_1{}^a$ [I>2σ(I)]	0.013	0.021
$wR_2{}^b$ [I>2σ(I)]	0.031	0.061
GOF	1.14	1.08

$^aR_1 = Σ||F_o|−|F_c||/Σ|F_o|$, $^bwR_2 = [Σw(|F_o|-|F_c|)^2/Σw|F_o|^2]^{1/2}$.

3 Results and Discussion

3.1 Structural Descriptions

3.1.1 Crystal structure of $BaCu_2(PO_4)_2(H_2O)$ (1)

The structure of compound **1** was first reported by Effenberger.[18] Single-crystal X-ray analysis reveals that **1** crystallizes in orthorhombic system with space group $P2_12_12_1$. As shown in Fig. S1†, there are two crystallographically different Cu atoms, which are all coordinated by five oxygen atoms forming $CuO_4(H_2O)$ square pyramids with four oxygen atoms from four different phosphate groups in the basal planes and water molecules occupying the apical positions. The Cu(1)–O bond lengths range from 1.911(2) to 2.490(2) Å, while the distances between Cu(2)–O are in the range of 1.922(2)–2.259(2) Å. Two independent crystallographic P atoms are tetrahedrally coordinated with four oxygen atoms, forming distorted PO_4 tetrahedrons with P(1)–O bond lengths varying from 1.505(2) to 1.584(2) Å and P(2)–O bond lengths scattering from 1.492(2) to 1.578(2) Å. The structural unit also consists of one water molecule bridging Cu(1) and Cu(2) and one Ba atom coordinated by eleven oxygen atoms forming a tricapped cube with the Ba–O bond lengths ranging from 2.727(2) to 3.214(2) Å. These crystallographic data coincide with results published in ref 18.

The main characteristic of the framework is that both $CuO_4(H_2O)$ square pyramids share their bevel edges and corners of basal planes to form alternate zigzag chains along *b* axis (Fig. 1a). The Cu–Cu separations are 3.192(4) and 3.259(3) Å, and the Cu–O–Cu bond angles are 84.32(4)°, 106.82(4)° and

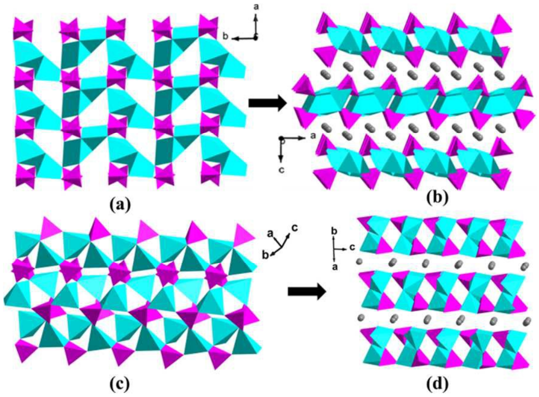

Fig. 1 (a) A 2D layer and (b) 3D framework for compound **1**. (c) A 2D layer and (d) 3D network for $BaCu_2(PO_4)_2$. Turquoise, Cu polyhedrons; Pink, PO_4 tetrahedrons; Gray balls, Ba^{2+} cations.

109.04(7)°. The chains are further linked through PO_4 tetrahedra by corner-sharing along *a* axis, expanding to layers that stack an *ABAB* sequence. Finally, the barium cations are located between layers (Fig. 1b). However, it is found that the CuO_5 square pyramids in corresponding anhydrous compound, $BaCu_2(PO_4)_2$, only share corners to form isolated chains, which are interconnected by PO_4 groups through corner- and edge-sharing to extend a 2D layer with an *AAAA* stacking sequence (Figs. 1c and 1d).[9a] The difference of coordination, linkage and stack fashion of Cu atoms result in different magnetism between compound **1** and $BaCu_2(PO_4)_2$.

3.1.2 Crystal structure of $Ba_2Cu(HPO_4)(PO_4)(OH)$ (2)

Compound **2** crystallizes in the monoclinic space group $P2_1/m$. The structure parameters and refinement information are provided in table 1. The asymmetric unit of **2** contains one Cu center, two independent Ba sites, two different P lattices, six oxygen atoms and one μ_3-OH^- anion. Except O1 and O4 atoms, the others have half of site occupancy factor in the crystallographically fundamental unit. The coordination environment of P, Cu and Ba atoms is displayed in Fig. S2†. It can be seen that the coordination geometries of P(1) and P(2) atoms are fairly common tetrahedra constructed from four oxygen atoms. The P(1)–O lengths are in the range of 1.531(6) to 1.550(4) Å and the P(2)–O distances vary from 1.513(5) to 1.636(6) Å. The longest bond length, P(2)–O(6) (1.636(6) Å), is assumed to be protonated.[4b] Moreover, the calculated bond valence sums (BVSs) show good agreement with the values of effective charge on Ba, Cu, P, O atoms, except for the O(6) (BVS = 1.04) and O(7) (BVS = 0.85), indicating a possible binding with protons. The existence of hydroxyl is also demonstrated by infrared spectroscopy (Fig. S6a† and text in part **3.2**). Consequently, two phosphate groups are formulated as $P(1)O_4$ and $P(2)O_3(OH)$, respectively, and O7 atom is an OH^- instead of an O^{2-} anion. The coexistence of hydroxyl and hydrogen phosphate within one compound is also found in $Co_3(HPO_4)_2(OH)_2$.[19] The Ba(1) and Ba(2) atoms are surrounded by ten and eleven oxygen atoms with Ba–O distances varying from 2.718(5) to 3.155(3) Å and from 2.588(6) to 3.210(3) Å, respectively.

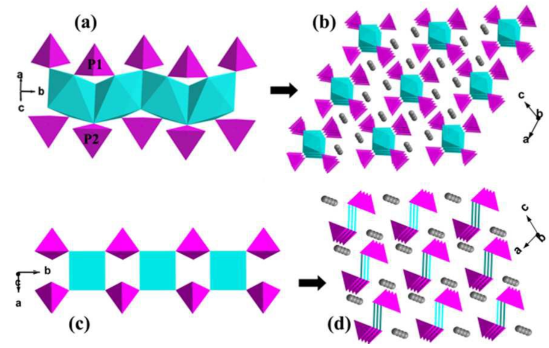

Fig. 2 (a) A 1D chain and (b) 3D framework in compound **2**. (c) A 1D chain and (d) 3D network in $Ba_2Cu(PO_4)_2$. Turquoise, Cu polyhedrons; Pink, PO_4 tetrahedrons; Gray balls, Ba^{2+} cations.

Each Cu atom is surrounded by six oxygen atoms, four from different PO_4 groups and the others from hydroxyls, forming a $CuO_4(OH)_2$ octahedron (Fig. S2†). The four shorter Cu–O bonds with lengths of 1.915(3) Å (x2, from OH^-) and 2.004(4) Å (x2, from $P(1)O_4$) constitute basal plane, while two longer Cu–O bonds with lengths of 2.486(3) Å from $P(2)O_3(OH)$ locate at the axial position of octahedron. The bond angles of Cu–O–Cu are equal to 72.4(3)° and 100.0(2)°. Fig. 2a shows that the $CuO_4(OH)_2$ octahedra are linked with each other by edge sharing to form an infinite chain running along *b* axis, giving a short Cu–Cu separation distance, 2.934(6) Å. The 3D framework structure of compound **2** is built up from infinite $[Cu(OH)PO_4]$ linear chains separated by barium cations (Fig. 2b). This arrangement lead to long Cu–Cu distances among chains along *a* axis (8.328(4) Å = *a*) and *c* axis (9.078(3) Å = *c*).

Compared with compound **2**, the CuO_4 squares in corresponding anhydrous compound, $Ba_2Cu(PO_4)_2$[10a], give rise to a $CuPO_4$ linear chain through Cu–O–P–O–Cu paths (Figs. 2c and 2d). Thus, there is no Cu–O–Cu superexchange. This linkage is also observed in another similar material $Ba_2Cu(PO_4)_2(H_2O)$.[18] The distinction among three similar compounds may be ascribed to their different structural features, such as space groups, coordination geometries of Cu atoms and the linkage of OH^- and H_2O. In addition, there are existence of hydrogen bonds in both compounds **1** and **2**, which are presented in Fig. S3 and Table S3.†

3.2 PXRD, IR and TG Analyses

According to the PXRD patterns shown in Figs. S4 and S5†, all peaks on the curves are indexed to the corresponding simulated ones, indicating the phase purity of two samples without any other impurities. From IR spectra (Fig. S6a†), both compounds contain many bands below 1500 cm^{-1}, which are consistent with different P–O, Cu–O and Ba–O modes. Two broad bands at about 1675 and 3381 cm^{-1} are observed in compound **1**, corresponding to water molecules. However, a rather sharp band is seen at 3626 cm^{-1} in compound **2**, emphasizing the existence of the OH^- groups. The thermal behavior of **1** and **2** is depicted in Fig. S6b†. It is clearly found that compound **1** begins to release the coordinated water molecules at 550 °C (found 3.94% and calcd 3.81%) and the

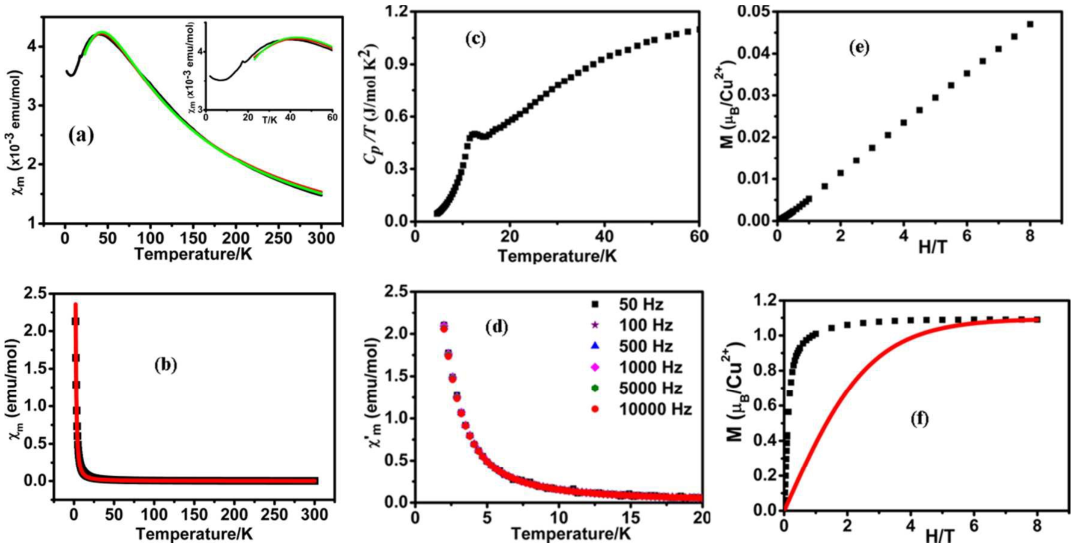

Fig. 3 (a) The χ_m vs T curve for **1** at 5 KOe. Green and red lines are fitting curves by eqs 1 and 2, 1 and 3, respectively. (b) The χ_m vs T curve for **2** under 1 KOe. Red line is fitted by eqs 1 and 4. (c) The C_p/T vs T curve for **1** at 0 T. (d) The ac susceptibilities at various frequencies for **2** with H_{dc} = 0 T and H_{ac} = 3 Oe. Isothermal magnetization curves measured at 2 K for **1** (e) and **2** (f). The red solid line in (f) is the S = 1/2 Brillouin function with g = 2.18.

following thermal behavior corresponds to the decomposition of the host skeleton at 880 °C. However, compound **2** dehydrates water molecules from hydroxyl groups at 480 °C (found 3.06% and calcd 3.29%) and then maintains stabilization. These features are good in agreement with the crystal structures.

3.3 Magnetic properties

Although the synthesis and structure of compound **1** was reported many years ago, magnetic properties have not been investigated yet. Magnetic susceptibilities for **1** and **2** were recorded on powder samples in the temperature range of 2–300 K. The temperature dependence of dc magnetic susceptibility is displayed in Fig. 3, and corresponding reciprocal susceptibility curves are shown in Fig. S7†. It can be seen that their magnetic behaviors are significantly different although both compounds consist of chains constructed from Cu polyhedra.

For compound **1**, the magnetic susceptibility exhibits a broad maximum around 40 K (Fig. 3a), a feature of one-dimensional antiferromagnets, corresponding to the onset of short-range AFM ordering. A small sharp peak at 17 K (inset in Fig. 3a) is observed with decreasing temperature, revealing long-range AFM ordering induced by interchain interactions. The slight increase at the lower temperature is attributed to the presence of a small amount of impurities or defects in the sample. However, the magnetic susceptibility of compound **2** (Fig. 3b) increases with decreasing temperature while a rapid increase is observed below 5 K, suggesting the presence of FM component. The high-temperature susceptibility data (150−300 K) obey the Curie–Weiss law, giving a C value of 0.46(3) emu K/mol and θ value of −45.82(1) K for **1** and a C value of 0.51(4) emu K/mol and θ value of 16.95(3) K for **2**. The effective magnetic moments of compounds **1** and **2** are calculated to be 1.93 μ_B and 2.01 μ_B, respectively, which are all a little larger than the spin-only value of 1.73 for S = 1/2 with g = 2. The negative and positive Weiss constants also confirm that the dominative interaction exchanges between Cu^{2+} ions are AFM in **1** and FM in **2**.

Fig. 3c shows the temperature dependence of specific heat divided by temperature of compound **1** in zero magnetic field. No peak is seen at 40 K and one broad small peak is found at 14 K, which is a little lower than the temperature position of the χ_m. No other anomalies are observed in the temperature range of 4.5–300 K. These features again demonstrate the existence of short-range ordering at 40K and long-range ordering at 14 K in compound **1**. In order to determine the long-range ordering temperature of compound **2**, we measured ac magnetic susceptibilities instead of specific heat because of the absence of enough sample. From Fig. 3d, it is obviously seen that the real part of ac magnetic susceptibilities are independent of frequencies and increase gradually without a peak. This fact implies that there is no long-range ordering above 2 K. In addition, Fig. S8† reveals the χ'_m values are strongly dependent on static magnetic field. A peak is obviously observed at 0.2 T and gradually transits to high temperature with increasing magnetic field to 8 T.

The behaviors of magnetization (M) as a function of applied field was measured at 2 K among 0–8 T. For **1** (Fig. 3e), the M values increase progressively to 0.047 μ_B at 8 T, which is much lower than the saturation value of 1 μ_B. The linear behavior of magnetization is in good agreement with the AFM ground state in the system. Isothermal magnetization curves for compound **2** were measured in the temperature range of 2 to 15 K, as shown in Figs. 3f and S9†. The M values at 2 K increase quickly at low field and trend to saturation at 1 T with the M value of 1.08 μ_B, slightly larger than the theoretical value of 1 μ_B. Also, the measured magnetization data increase much faster than expected values calculated from Brillouin

Table 2 The geometrical parameters of main interactions for $BaCu_2(PO_4)_2(H_2O)$ and $Ba_2Cu(HPO_4)(PO_4)(OH)$.

compound	*J*	pathway	bond length (Å)	angle (°)
$BaCu_2(PO_4)_2(H_2O)$	J_1	1	Cu(1)–O(4) = 1.998, Cu(2)–O(4) = 2.005	Cu(1)–O(4)–Cu(2) = 109.04
	J_2	1	Cu(1)–O(5) = 2.014, Cu(2)–O(5) = 1.961	Cu(1)–O(5)–Cu(2) = 106.82
	J_3	1	Cu(2)–O(5) = 1.961, Cu(1)–O(6) = 1.912 O(5)–O(6) = 2.512	Cu(1)–O(6)–O(5) = 122.53 O(6)–O(5)–Cu(2) = 80.16
		2	Cu(2)–O(2) = 1.987, Cu(1)–O(4) = 1.998 O(2)–O(4) = 2.522	Cu(1)–O(4)–O(2) = 86.64 O(4)–O(2)–Cu(2) = 114.01
	J_4	1	Cu(1)–O(1) = 1.912, Cu(2)–O(4) = 2.005 O(1)–O(4) = 2.514	Cu(1)–O(1)–O(4) = 124.01 O(1)–O(4)–Cu(2) = 85.77
		2	Cu(1)–O(5) = 2.014, Cu(2)–O(7) = 1.922 O(5)–O(7) = 2.500	Cu(1)–O(5)–O(7) = 90.48 O(5)–O(7)–Cu(2) = 122.36
	J_5	1	Cu(2)–O(5) = 1.961, Cu(2)–O(7) = 1.922 O(5)–O(7) = 2.500	Cu(2)–O(5)–O(7) = 134.80 O(5)–O(7)–Cu(2) = 122.36
		2	Cu(2)–O(2) = 1.987, Cu(2)–O(4) = 2.005 O(2)–O(4) = 2.522	Cu(2)–O(2)–O(4) = 114.01 O(2)–O(4)–Cu(2) = 139.20
	J_6	1	Cu(1)–O(5) = 2.014, Cu(1)–O(6) = 1.912 O(5)–O(6) = 2.512	Cu(1)–O(5)–O(6) = 140.10 O(5)–O(6)–Cu(1) = 122.50
		2	Cu(1)–O(1) = 1.912, Cu(1)–O(4) = 1.998 O(1)–O(4) = 2.514	Cu(1)–O(1)–O(4) = 124.01 O(1)–O(4)–Cu(1) = 138.39
$Ba_2Cu(HPO_4)(PO_4)(OH)$	*J*	1	Cu(1)–O(7)H = 1.915 (x 2)	Cu(1)–O(7)H–Cu(1) = 100.00

function with S = 1/2 and g = 2.18. This result also indicates the main interaction between nearest-neighbor Cu atoms is FM. No hysteresis loop and remanent magnetization at 0 T can be observed in both compounds.

3.4 Discussion

It is found that both bond lengths and angles play important role on the sign and strength of magnetic couplings. The longer axial Cu–O bonds could be negligible. Thus, all polyhedra in both compounds change to squares where the $\mathbf{d}_{x^2-y^2}$ orbitals occupied by Cu spins are resided. In general, the main couplings are controlled by direct Cu–O–Cu superexchanges. However, the supersuperexchange interactions mediated by Cu–O···O–Cu paths where the O···O represents an edge of PO_4 tetrahedron will have considerable value when CuO_4 squares and PO_4 groups locate on the suitable position. For example, the degree of couplings will increase with decreasing the O···O distance, and the Cu–O···O angle in the vicinity of 132° is optimal.[11a] For compounds **1** and **2**, the dominant magnetic exchange paths are shown in Fig. 4, and corresponding geometrical parameters are summarized in Table 2.

To estimate the strength of intrachain couplings, we fit the $\chi(T)$ data by following equations.

$$\chi = \chi_0 + \frac{C_{\mathrm{imp}}}{T - \theta_{\mathrm{imp}}} + \chi_{\mathrm{chain}} \qquad (1)$$

Where χ_0 represents the temperature independent term containing Van Vleck paramagnetic and the diamagnetic contributions, C_{imp} and θ_{imp} are Curie constant and Weiss temperature from free spins and impurities, χ_{chain} is the intrachain magnetic contribution.

For compound **1**, there are six different interactions (Fig. 4a). From results reported in ref 11a, J_3 and J_4 could be negligible. If J_1 and J_2 are dominant intrachain constants and J_5 and J_6 are interchain interactions, the alternating chains model is more reasonable although the bong lengths and angles of J_1 and J_2 paths are similar. The degree of J_1 is a little larger than J_2 due to the slightly bigger angle (109.04° vs 106.82°). So χ_{chain} is fitted by equation (2).[20]

$$\chi_{\mathrm{chain}} = \frac{Ng^2\beta^2 e^{-A(\alpha)/t}}{4\kappa_B T}\rho(\alpha, t) \qquad (2)$$

where $\alpha = J_2/J_1$ ($J_2 < J_1$), $t = \kappa_B T/J_1$, *N*, g, β and k_B represent Avogadro number, Lande factor, Bohr magneton and Boltzmann constant, respectively. The complete information of equation (2) can be found in equation (56) of ref 20.

The second case is that J_5 and J_6 are predominant intrachain interactions while J_1 and J_2 are responsible for interchain constants. So, two uniform chains are constructed from $Cu(1)O_4$ along *a* axis and $Cu(2)O_4$ along *b* axis, respectively. We consider J_5 equal to J_6 in terms of their similar geometries. Thus, the measured data can be fitted by uniform chain model using equation (3).[20]

$$\chi_{chain} = \frac{Ng^2\beta^2}{4\kappa_B T}\frac{1+\sum_{n=1}^{5} N_n/t^n}{1+\sum_{n=1}^{6} D_n/t^n} \qquad (3)$$

where $t = \kappa_B T/J$, the parameters could be found in equation (50) of ref 20.

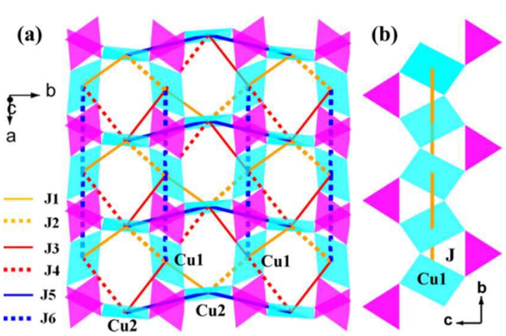

Fig. 4 The dominative magnetic couplings in **1** (a) and **2** (b).

The fitted results from equations (2) and (3), respectively, are listed in Table 3. The poor fitting curves shown in Fig 3a indicate that both alternating and uniform models should be inadequacy although the fitted values look like reasonable. On the basis of crystal structure and magnetic analysis, we suggest the strengths of couplings involving Cu–O–Cu and Cu–O···O–Cu paths are comparative to get rid of isolated 1D chain model, resulting in a 2D magnetic topology along *ab* plane. Furthermore, these interactions are strong enough to enhance a 3D AFM ordering at 14 K.[12,21] However, there is no 3D ordering above 2 K in $BaCu_2(PO_4)_2$ and the susceptibility can be fitted better by spin ladder than alternating chain model.[9a,9b] The widely different magnetic behaviors between **1** and $BaCu_2(PO_4)_2$ result from different crystal structures (Fig. 1).

However, in compound **2**, there is only one intrachain exchange constant mediated by the path Cu(1)–O(7)H–Cu(1) (*J*). Thus, χ_{chain} is fitted to the model of 1D uniform Heisenberg ferromagnetic chain with equation (4).[22]

$$\chi_{\mathrm{chain}} = \frac{Ng^2\beta^2}{4\kappa_B T}\left[1 + \left(\frac{J}{\kappa_B T}\right)\right] \qquad (4)$$

The meanings of *N*, g, β and k_B are the same as those in equation (2). The best fitting parameters are presented in Table 3.

Fig. S10† shows $\chi_m T$ in compound **2** continues to increase at low temperature. This phenomenon is the same as $SrCuV_2O_7$,[14] but is different from $BaCuV_2O_7$[14] and $BaCu_2Ge_3O_9 \cdot H_2O$,[15] where $\chi_m T$ exhibit a maximum at 3 k and 8 k, respectively. The J/κ_B (4.62 K) in $SrCuV_2O_7$ is much lower than that in **2** (J/κ_B = 22.06 K). This is attributed to no direct Cu–O–Cu exchange paths. However, $SrCuV_2O_7$ undergoes long-range AFM ordering at 1.36 K and a spin flop transition at 500 Oe. These results demonstrate the exchange interactions among 1D FM chains are AFM. To obtain more magnetic information of compound **2**, susceptibilities were measured under various applied fields from 0.001 T to 8 T in the temperature range of 2–30 K. As seen in Fig. S11†, the susceptibility decrease with decreasing temperature at 0.001 T, while the χ_m values increase with decreasing temperature above 0.001 T. Moreover, the values at 2 K increase with increasing external fields

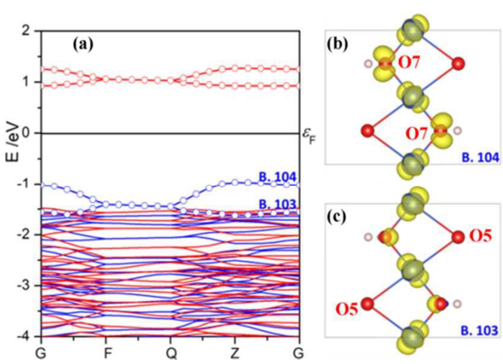

Fig. 5 (a) Band structure of compound 2 from GGA+U calculation. Blue (red) lines correspond to up-spin (down-spin) bands. (b) and (c) Band-decomposed charge density figures corresponding to the selected band 104 (B. 104) and band 103 (B. 103), respectively.

Table 3 The fitting results for compounds $BaCu_2(PO_4)_2(H_2O)$ and $Ba_2Cu(HPO_4)(PO_4)(OH)$.

parameters	$BaCu_2(PO_4)_2(H_2O)$		$Ba_2Cu(HPO_4)(PO_4)(OH)$
	eqs 1 and 2	eqs 1 and 3	eqs 1 and 4
χ_0 (emu/mol)	0.88×10^{-4}	1.42×10^{-4}	-1.38×10^{-4}
C_{imp} (emu K/mol)	2.25×10^{-3}	3.46×10^{-3}	4.06×10^{-4}
θ_{imp} (K)	1.33	–1.27	1.07
g	2.25	2.23	2.04
J/κ_B (K)	J_1/κ_B –68.99 (AFM)	J_5/κ_B –68.60 (AFM)	22.06 (FM)
α	0.98		

to 0.1 T, above of which the susceptibilities drop with increasing applied fields to 8T. In addition, the low-field dependence susceptibilities (Fig. S11a†) persist up to 30 K, implying the presence of a FM impurity. These data further clarify no magnetic ordering is observed above 2 K.

A rough rule predicts the exchange constant is FM for angles less than 95° and usually AFM for angles larger than 95°.[23] The simple rule is in good agreement with the observations in **1**. However, it does not work for **2**. In order to understand the origination of intrachain FM coupling in **2**, we performed first-principle electronic-structure calculations based on the generalized-gradient approximation[24] including the electron-electron Coulomb interactions[25] (*GGA+U*, *U* = 4.0 eV as in the case of other cuprates[26]) and the projector-augmented wave method[27] employed in VASP Program.[28] Fig. 5 shows the band structure and the decomposed charge densities at the highest occupied bands, band-104 and band-103. We find that the intrachain FM couplings propagate along Cu(1)–O(7)H–Cu(1) pathways by $\mathbf{d}p\sigma$ correlation superexchange in spite of the angle equal to 100.00°.[29] In fact, the bigger angles also can propagate FM interaction in some materials. For example, in a molecule magnet with formula of $Cu_4C_{52}H_{68}N_{22}O_{33}$, the intramolecular exchange constants are FM between Cu centers despite of extremely big Cu–O–Cu angles ranging from 139.2 to 140.6°.[30]

4 Conclusions

Two barium copper phosphates, $BaCu_2(PO_4)_2(H_2O)$ (**1**) and $Ba_2Cu(HPO_4)(PO_4)(OH)$ (**2**), were successfully prepared through one-pot hydrothermal reaction. In compound **1**, $CuO_4(H_2O)$ square pyramids constitute alternating chains along *b* axis by alternative corner and edge sharing, while $CuO_4(OH)_2$ octahedra in compound **2** form uniform chains along *b* axis through edge sharing. This results in significantly different magnetic behaviors. The measurements of susceptibility, magnetization and specific heat evidence that compound **1** shows typical 1D AFM characterizations with a short-range ordering around 40 K and a long-range ordering at 14 K, and compound **2** do not appear long-range ordering above 2 K with FM intrachain interactions. The first principle calculations demonstrate the intrachain FM couplings in **2** are ascribed to $\mathrm{d}p\sigma$ correlation superexchanges through Cu(1)–O(7)H–Cu(1) paths.

Acknowledgement

This work is supported by National Basic Research Program of China (No. 2012CB921701).

References

1 (a) F. D. M. Haldane, *Phys. Rev. Lett*, 1983, **50**, 1153; (b) H. C. Lu, T. Yamamoto, W. Yoshimune, N. Hayashi, Y. Kobayashi, Y. Ajiro and H. Kageyama, *J. Am. Chem. Soc*, 2015, **137**, 9804; (c) A. N. Vasil'ev, M. M. Markina and E. A. Popova, *Low Temp Phys*, 2005, **31**, 203; (d) V. Zapf and M. Jaime, *Rev Mod Phys*, 2014, **86**, 563.

2 (a) H. Rosner, M. D. Johannes, S. L. Drechsler, M. Schmitt, O. Janson, W. Schnellea, W. Liu, Y. X. Huang and R. Kniep, *Sci Technol Adv Mat*, 2007, **8**, 352; (b) E. Dagotto and T. M. Rice, *Science*, 1996, **271**, 618; (c) J. Schlappa, K. Wohlfeld, K. J. Zhou, M. Mourigal, M. W. Haverkort, V. N. Strocov, L. Hozoi, C. Monney, S. Nishimoto, S. Singh, A. Revcolevschi, J. S. Caux, L. Patthey, H. M. Rønnow, J. van den Brink and T. Schmitt, *Nature*, 2012, **485**, 82.

3 (a) M. Hase, I. Terasaki and K. Uchinokura, *Phys. Rev. Lett*, 1993, **70**, 3651; (b) Y. Sasago, M. Hase, K. Uchinokura, M. Tokunaga and N. Miura, *Phys. Rev. B*, 1995, **52**, 3533.

4 (a) S. Lebernegg, A. A. Tsirlin, O. Janson and H. Rosner, *Phys. Rev. B*, 2013, **88**, 224406; (b) R. Baies, V. Caignaert, V. Pralong and B. Raveau, *Inorg. Chem*, 2005, **44**, 2376; (c) M. Hase, M. Kohno, H. Kitazawa, N. Tsujii, O. Suzuki, K. Ozawa, G. Kido, M. Imai and X. Hu, *Phys. Rev. B*, 2006, **73**, 104419.

5 (a) H. Kikuchi, Y. Fujii, M. Chiba, S. Mitsudo, T. Idehara, T. Tonegawa, K. Okamoto, T. Sakai, T. Kuwai and H. Ohta, *Phys. Rev. Lett*, 2005, **94**, 227201; (b) M. Fujihala, H. Koorikawa, S. Mitsuda, M. Hagihala, H. Morodomi, T. Kawae, A. Matsuo and K. Kindo, *J. Phys. Soc. Jpn*, 2015, **84**, 073702.

6 (a) X. Zhang, S. Nishihara, Y. Nakano, E. Yoshida, C. Kato, X. M. Ren, K. Y. Maryunina and K. Inoue, *Dalton Trans*, 2014, **43**, 12974; (b) B. Koteswararao, S. Salunke, A. V. Mahajan, I. Dasgupta and J. Bobroff, *Phys. Rev. B*, 2007, **76**, 052402.

7 (a) H. Vanherzeele, *Appl. Opt*, 1988, **27**, 3608; (b) Z. Y. Bi, X. D. Zhang, W. He, D. D. Min and W. S. Zhang, *RSC Adv*, 2013, **3**, 19744; (c) G. Wang, B. B. Huang, X. C. Ma, Z. Y. Wang, X. Y. Qin, X. Y. Zhang, Y. Dai and M. H. Whangbo, *Angew. Chem. Int. Ed*, 2013, **52**, 4810.

8 (a) A. Boukhari, A. Moqine and S. Flandrois, *Mat. Res. Bull*, 1986, **21**, 395; (b) M. Drillon, M. Belaiche, P. Legoll, J. Aride, A. Boukhari and A. Moqine, *J. Magn. Magn. Mater*, 1993, **128**, 83; (c) M. Matsuda, K. Kakurai, A. A. Belik, M. Azuma, M. Takano and M. Fujita, *Phys. Rev. B*, 2005, **71**, 144411; (d) S. Yamamoto and J. Ohara, *Phys. Rev. B*, 2007, **76**, 014409.

9 (a) A. Moqine, A. Boukhari and J. Darriet, *J. Solid State Chem*, 1993, **107**, 362; (b) Aripin, S. Mitsudo, T. Idehara and M. Mekata, *J. Matematika. Dan. Sains*, 2003, **8**, 7; (c) M. Mekata, T. Hanabata, K. Nakaya and Y. Ajiro, *J. Magn. Magn. Mater*, 2001, **226–230**, 410; (d) A. A. Belik, M. Azuma, A. Matsuo, M. H. Whangbo, H. J. Koo, J. Kikuchi, T. Kaji, S. Okubo, H. Ohta, K. Kindo and M. Takano, *Inorg. Chem*, 2005, **44**, 6632; (e) T. Kaji, S. Okubo, H. Ohta, Y. Inagaki, A. A. Belik, M. Azuma and M. Takano, *J. Phys Chem Solids*, 2005, **66**, 2068; (f) A. A. Belik, M. Azuma, A. Matsuo, T. Kaji, S. Okubo, H. Ohta, K. Kindo and M. Takano, *Phys. Rev. B*, 2006, **73**, 024429.

10 (a) K. M. S. Etheredge and S. J. Hwu, *Inorg. Chem*, 1996, **35**, 1474; (b) A. A. Belik, S. Uji, T. Terashima and E. T. Muromachi, *J. Solid State Chem*, 2005, **178**, 3461; (c) A. A. Belik, M. Azuma and M. Takano, *J. Solid State Chem*, 2004, **177**, 883.

11 (a) A. A. Belik, M. Azuma and M. Takano, *Inorg. Chem*, 2003, **42**, 8572; (b) A. Boukhari, A. Moqine, S. Flandrois, *J. Solid State Chem*, 1990, **87**, 251.

12 A. A. Belik, M. Azuma and M. Takano, *Inorg. Chem*, 2005, **44**, 7523.

13 For examples: (a) R. D. Willett, C. P. Landee, R. M. Gaura, D. D. Swank, H. A. Groenendijk and A. J. van Duyneveldt, *J. Magn. Magn. Mater*, 1980, **15–18**, 1055; (b) R. Hoogerbeets, E. H. Abu Bakr and A. J. Van Duyneveldt, *Physica B+C,* 1985, **128**, 161; (c) H. A. Algra, L. J. de Jongh, W.J. Huiskamp and R. L. Carlin, *Physica B+C,* 1977, **92**, 187; (d) C. P. Landee and R. D. Willett, *Phys. Rev. Lett,* 1979, **43**, 463; (e) M. B. Ritter, J. E. Drumheller, T. M. Kite, L. O. Snively and K. Emerson, *Phys. Rev. B,* 1983, **28**, 4949; (f) D. D. Swank, C. P. Landee and R. D. Willett, *Phys. Rev. B,* 1979, **20**, 2154; (g) R. D. Willett, C. Landee and D. D. Swank, *J. Appl. Phys,* 1978, **49**, 1329; (h) S. K. Satija, J. D. Axe, R. Gaura, R. Willett and C. P. Landee, *Phys. Rev. B,* 1982, **25**, 6855; (i) K. Kopinga, W. J. M. de Jonge, M. Steiner, G. C. de Vries and E. Frikkee, *Phys. Rev. B*, 1986, **34**, 4826; (j) D. N. Haines and J. E. Drumheller, *Phys. Rev. Lett.* 1987, **58**, 2702; (k) L. K. Thompson, S. S. Tandon, F. Lloret, J. Cano and M. Julve, *Inorg. Chem*, 1997, **36**, 3301.

14 A. A. Belik, M. Azuma, A. Matsuo, K. Kindo and Mikio Takano, *Inorg. Chem*, 2005, **44**, 3762.

15 P. Brandão, M. S. Reis, Z. Gai and A. M. D. Santos, *J. Solid State Chem*, 2013, **198**, 39.

16 (a) D. Boldrin and A. S. Wills, *J. Mater. Chem. C*, 2015, **3**, 4308; (b) T. T. Zhu, W. Sun, Y. X. Huang, Z. M. Sun, Y. M. Pan, L. Balents and J. X. Mi, *J. Mater. Chem. C*, 2014, **2**, 8170.

17 G. M. Sheldrick, *SHELXL-97. Program for refinement of crystal structures*, University of Göttingen, Göttingen, Germany, 1997.

18 H. Effenberger, *J. Solid State Chem*, 1999, **142**, 6.

19 J. L. Pizarro, G. Villeneuve, P. Hagenmuller and A. L. Ball, *J. Solid State Chem*, 1991, **92**, 273.

20 D. C. Johnston, R. K. Kremer, M. Troyer, X. Wang, A. Klümper, S. L. Bud'ko, A. F. Panchula and P. C. Canfield, *Phys. Rev. B*, 2000, **61**, 9558.

21 (a) R. David, H. Kabbour, S. Colis, A. Pautrat, E. Suard and O. Mentré, *J. Phys. Chem. C*, 2013, **117**, 18190; (b) H. B. Yahia, D. Mori, M. Shikano, H. Kobayashi and Y. Inaguma, *Dalton Trans*, 2014, **43**, 13630.

22 K. Takeda, K. Konishi, K. Nedachi and K. Mukai, *Phys. Rev. Lett*, 1995, **74**, 1673.

23 Y. Mizuno, T. Tohyama, S. Maekawa, T. Osafune, M. Motoyama, H. Eisaki and S. Uchida, *Phys. Rev. B*, 1998, **57**, 5326.

24 J. P. Perdew, K. Burke and M. Ernzerhof, *Phys. Rev. Lett*, 1996, **77**, 3865.

25 (a) G. Kresse and J. Hafner, *Phys. Rev. B*, 1993, **48**, 13115; (b) G. Kresse and J. Furthmüller, *Phys. Rev. B*, 1996, **54**, 11169; (c) G. Kresse and J. Furthmüller, *Comput. Mater. Sci*, 1996, **6**, 15.

26 H. Wu, Q. Q. Zheng, X. G. Gong and H. Q. Lin, *J. Phys.: Condens. Matter*, 1999, **11**, 4637.

27 (a) P. E. Blöchl, *Phys. Rev. B*, 1994, **50**, 17953; (b) G. Kresse, and D. Joubert, *Phys. Rev. B*, 1999, **59**, 1758.

28 (a) V. I. Anisimov, F. Aryasetiawan and A. I. Liechtenstein, *J. Phys. Condens. Matter*, 1997, **9**, 767; (b) S. L. Dudarev and G. A. Botton, *Phys. Rev. B*, 1998, **57**, 1505.

29 J. B. Goodenough, *Magnetism and the Chemical Bond*. Interscience-Wiley, New York, 1963; Chapter 3, pp 181.

30 Z. Q. Xu, L. K. Thompson and D. O. Miller, *J. Chem. Soc., Dalton Trans*, 2002, 2462.

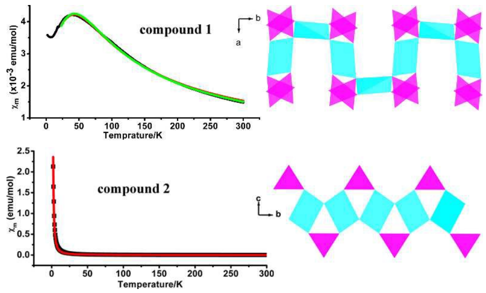

Compound **1** contains alternating chains with 3D ordering at 14 K, while **2** consists of uniform chains without 3D ordering above 2 K.